Impact of p-GaN Thermal Damage and Barrier Composition on Semipolar Green Laser Diodes

Matthew T. Hardy, Feng Wu, Chia-Yen Huang, Yuji Zhao, Daniel F. Feezell, Shuji Nakamura, James S. Speck, and Steven P. DenBaars, *Fellow, IEEE*

***Abstract*— Dark triangle defects (DTDs) are common nonradiative defects in semipolar ($20\bar{2}1$) oriented green quantum wells (QWs), commonly used in green laser diodes (LDs). We show that DTDs do not appear "as-grown," and DTD size depends strongly on post-QW-growth annealing time and temperature. Using low temperature p-GaN, we prevent catastrophic QW damage and directly compare LDs with GaN and AlGaN containing barriers. The GaN barrier LD exhibited a lasing wavelength of 511 nm, reduced operating voltage, and the lowest threshold current density, likely due to enhanced optical confinement factor and the elimination of very low growth temperature AlGaN in the active region.**

***Index Terms*— Quantum well lasers, green laser diodes, semipolar GaN, epitaxial defects, thermal stability.**

I. Introduction

GROWTH of green lasers diodes (LDs) on semipolar (SP) growth orientations of GaN has several potential advantages over traditional *c*-plane oriented devices, namely a reduction in polarization-related electric fields in the quantum wells (QWs) leading to higher radiative recombination rates [1]. Unbalanced biaxial stress in the InGaN QWs for reduced symmetry SP orientations leads to a splitting of the top two valence bands, and is predicted to lead to enhanced gain on SP growth orientations relative to *c*-plane [2]. In addition, SP LDs may have higher differential efficiency and more linear gain versus current behavior relative to *c*-plane, making them more tolerant to optical loss and better suited to high power applications [2], [3].

In spite of the remarkable recent progress made on green LDs [4], [5], very little has been published about epitaxial development. Dark triangle defects (DTDs) are common defects in green SP LD structures that dramatically reduce luminescence efficiency and thus prevent lasing [3], [6].

Manuscript received May 13, 2013; revised September 17, 2013; accepted October 11, 2013. Date of publication November 5, 2013; date of current version December 13, 2013. This work was supported in part by the Solid State Lighting and Energy Center, in part by the UCSB Materials Research Laboratory facilities which are funded by the NSF Materials Research Science and Engineering Center Program under Grant DMR-1121053, in part by the UCSB nanofabrication facility, and in part by the NSF funded NNIN network.

M. T. Hardy, F. Wu, C.-Y. Huang, Y. Zhao, S. Nakamura, J. S. Speck, and S. P. DenBaars are with the Materials Department, University of California, Santa Barbara, CA 93106-5050 USA (e-mail: mthardy@engineering.ucsb.edu; feng.wu@mrl.ucsb.edu; chiayen@umail.ucsb.edu; yujizhao@engineering.ucsb.edu; shuji@engineering.ucsb.edu; speck@mrl.ucsb.edu; denbaars@engineering.ucsb.edu).

D. F. Feezell is with the Department of Electrical and Computer Engineering, University of New Mexico, Albuquerque, NM 87106-4343 USA (e-mail: dfeezell@chtm.unm.edu).

Color versions of one or more of the figures in this letter are available online at http://ieeexplore.ieee.org.

Digital Object Identifier 10.1109/LPT.2013.2288927

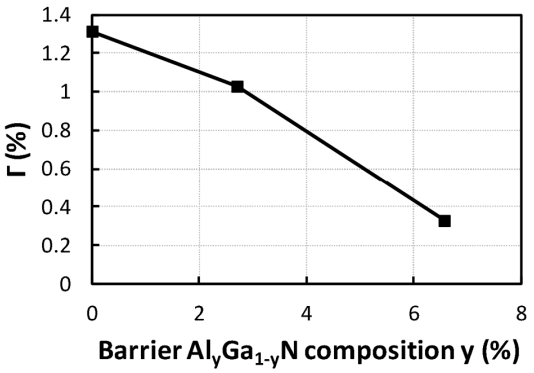

Fig. 1. Calculated dependence of confinement factor on the AlN fraction in the barriers for a 520 nm GaN clad LD with InGaN waveguiding layers.

Macroscopic non-radiative defects have also been observed in *c*-plane oriented green LD structures [7]. AlGaN barriers can suppress DTDs that form in ($20\bar{2}1$) oriented LD structures having $In_xGa_{1-x}N$ QW compositions necessary for lasing in the green spectrum [6]. However, AlGaN barriers decrease the optical confinement factor (Γ) by reducing the active region average index, and may lead to other growth related issues including poor material quality at the very low temperatures necessary for green InGaN QW growth. Confinement factor calculations using commercially available FIMMWAVE software are given in Fig. 1 for a GaN clad LD structure [8]. The simulated structure consisted of a three period multi-QW (MQW) active region with 2.7 nm thick QWs, 10 nm barriers, a 10 nm $Al_{0.2}Ga_{0.8}N$ electron blocking layer (EBL), symmetric 30 nm $In_{0.08}Ga_{0.92}N$ waveguiding layers and GaN cladding. InGaN and AlGaN index values were taken from [9] and [10], respectively. Clearly, increasing the $Al_yGa_{1-y}N$ composition y in the barriers decreases the optical confinement factor, leading to increased lasing threshold current density (J_{th}) for a GaN clad LD with AlGaN barriers.

In this letter, we studied the effect of post-QW growth time and temperature on DTD formation to understand the factors controlling their formation, and investigate the nature of DTDs using transmission electron microscopy (TEM). We then use these observations to grow and fabricate green LDs with GaN barriers and compare them to LDs with AlGaN barriers.

II. Experimental

All samples in this letter were grown by atmospheric pressure horizontal flow metalorganic chemical vapor deposition on free standing ($20\bar{2}1$) GaN substrates with threading dislocation densities of approximately 5×10^6 cm^{-2}, provided

1041-1135 © 2013 IEEE

by Mitsubishi Chemical Corporation. A series of samples with 2.7 nm thick QWs and 10 nm thick GaN barriers was grown with different post-QW thermal profiles. The first sample contained a 600 nm n-GaN buffer layer followed by the MQW active region and a 10 nm GaN cap grown at approximately 760 °C. The remaining samples were simple light-emitting diode (LED) structures with the same buffer and MQW active region, a 10 nm $Al_{0.2}Ga_{0.8}N$ EBL, and 15 minutes of p-GaN grown at 920 °C, giving approximately 150 nm of p-GaN. Following p-GaN growth, the samples were annealed *in-situ* in a N_2/NH_3 ambient similar to that supplied during the p-GaN growth, but substituting N_2 instead of the H_2 carrier gas normally used to prevent etching of the p-GaN surface. The anneal temperature was the same as the p-GaN growth temperature (920 °C) and the anneal times were 0, 15, 30 and 60 minutes, giving a total post-QW time at 920 °C of 15, 30, 45 and 75 minutes. All temperatures were measured from a thermocouple placed inside the susceptor and were approximately 50–100 °C greater than the sample surface temperature. Defect morphology in the QWs was examined using fluorescence microscopy (FLM) with an excitation band from 450–490 nm and a 520 nm longpass filter.

A second series of full LD structures was grown with post-QW growth temperature varied among 840, 860 and 920 °C. The GaN clad LD structure included a 1.2 μm n-GaN buffer layer, n- and p-$In_{0.08}Ga_{0.92}N$ waveguiding layers approximately 30 nm thick, and 700 nm p-GaN cladding. Trimethylgallium (TMGa) was used as the Ga precursor for the n-GaN growth, while triethylgallium (TEGa) and trimethylindium (TMIn) were used for the Ga and In precursors for the InGaN waveguiding layers, QWs, barriers and p-GaN. TEGa was used as the Ga precursor in the p-GaN as a precaution to prevent excessive carbon incorporation in the relatively low temperature p-GaN growth [11]. For comparison to the previous experiment, the total p-InGaN and p-GaN growth time was 61.5 minutes, and the LD structure employed the same active region and EBL used above. The samples were examined using FLM, and TEM analysis was conducted on a similar LD structure having GaN barriers with p-GaN grown at 920 °C to investigate the microstructure of the DTDs.

Finally, a third series was grown to assess the impact of AlGaN barriers on device performance using the same GaN clad LD structure with a p-GaN growth temperature of 890 °C. Three samples were grown with $Al_yGa_{1-y}N$ barrier compositions of $y = 0$ (GaN barriers), 0.027 and 0.066. The AlGaN composition was estimated from X-ray diffraction measurements of a calibration sample which was grown separately. Devices from the AlGaN barrier series were processed into ridge waveguide LDs via a self-aligned lift-off process to etch the ridges and open vias in the SiO_2, using the same photoresist for the ridge etch mask and SiO_2 liftoff. Pd/Au p-contacts were then deposited and facets were formed using Cl_2 reactive-ion etching. Al/Au contacts were deposited on the back side of the wafer to serve as a common n-contact.

III. Results

Figure 2(a–e) shows fluorescence micrographs depicting the impact of *in-situ* post-growth anneal time of green

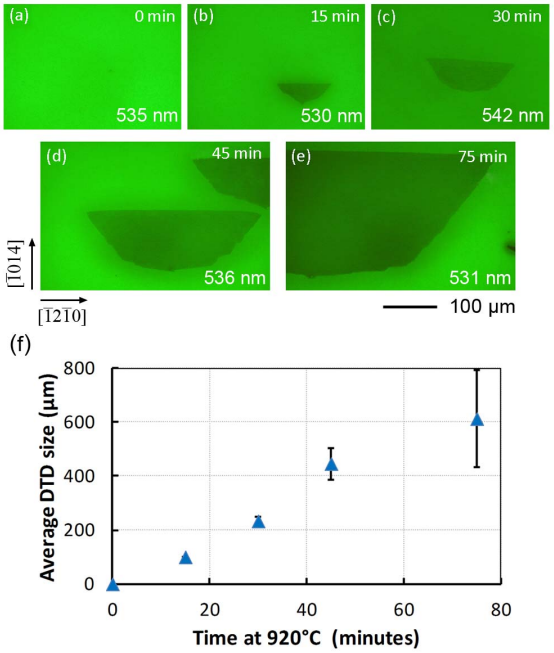

Fig. 2. Fluorescence micrographs of (a) a 3× QW structure with a 10 nm UID GaN cap, and LED structures with 15 minutes (150 nm) of p-GaN grown at 920 °C followed by an additional (b) 0 minute, (c) 15 minute, (d) 30 minute and (e) 60 minute *in-situ* anneal at 920 °C. The total time at 920 °C is inset in the top right corner and the PL peak wavelength is inset in the bottom right corner. (f) Dependence of average DTD size on total time at temperature, with error bars representing one standard deviation.

(20$\bar{2}$1) QWs. PL wavelengths of these samples varied from 530 to 542 nm due to run-to-run variation and are inset in the lower right corner of each image. The total time at temperature is inset in the top right of each image. The sample with no post-QW anneal showed no evidence of DTDs. As the total anneal time was increased from 15 to 75 minutes, DTDs appeared and increased significantly in size. The maximum DTD size for the 75 minute sample was 990 μm, measured as the maximum width parallel to the a-direction. The average DTD size as a function of total anneal time is given in Fig. 2(f), with error bars representing one standard deviation. DTD density does not appear to depend on anneal time, in contrast with the behavior of DTD size.

FLM images of GaN clad LD structures with different post-QW growth temperatures are given in Fig. 3. Electroluminescence wavelength measured at 20 A/cm^2 is inset in each image, along with the post-QW growth temperature. The size of the DTDs was strongly dependant on growth temperature, similar to the dependence on growth time. For the 840 °C sample, and the maximum DTD size was approximately 250 μm as opposed to the 920 °C sample where over half the sample was completely dark due to DTDs and the largest individual defect was over 1 mm wide parallel to the a-direction. Average DTD size as a function of p-GaN temperature is given in Fig. 3(d).

Figure 4 shows a two beam diffraction contrast TEM image with diffraction vector $g = 0002$ and zone axis B = [$\bar{1}2\bar{1}0$] from a DTD region in a GaN LD structure with GaN barriers and a p-GaN temperature of 920 °C. Voids and basal plane stacking faults (BPSFs) are visible in the image, and both types

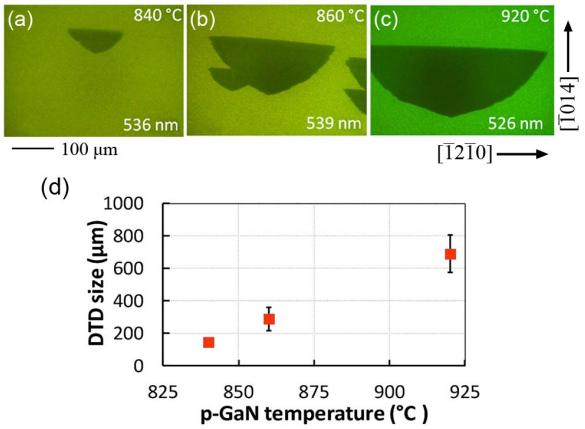

Fig. 3. Fluorescence micrographs of GaN clad LD structures with p-InGaN and p-GaN growth temperatures of (a) 840 °C, (b) 860 °C and (c) 920 °C, with the electroluminescence wavelength inset in the lower right corner. (d) Dependence of average DTD size on p-GaN temperature, with error bars representing one standard deviation.

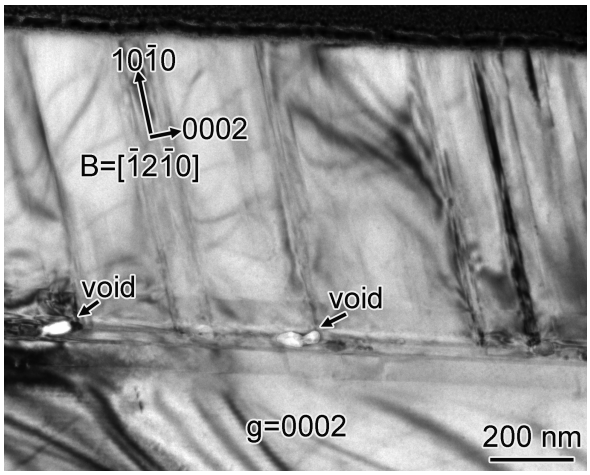

Fig. 4. Two beam diffraction contrast image taken in the DTD area of a LD structure. The DTDs contains voids and basal plane stacking faults which initiate in the InGaN/GaN active region.

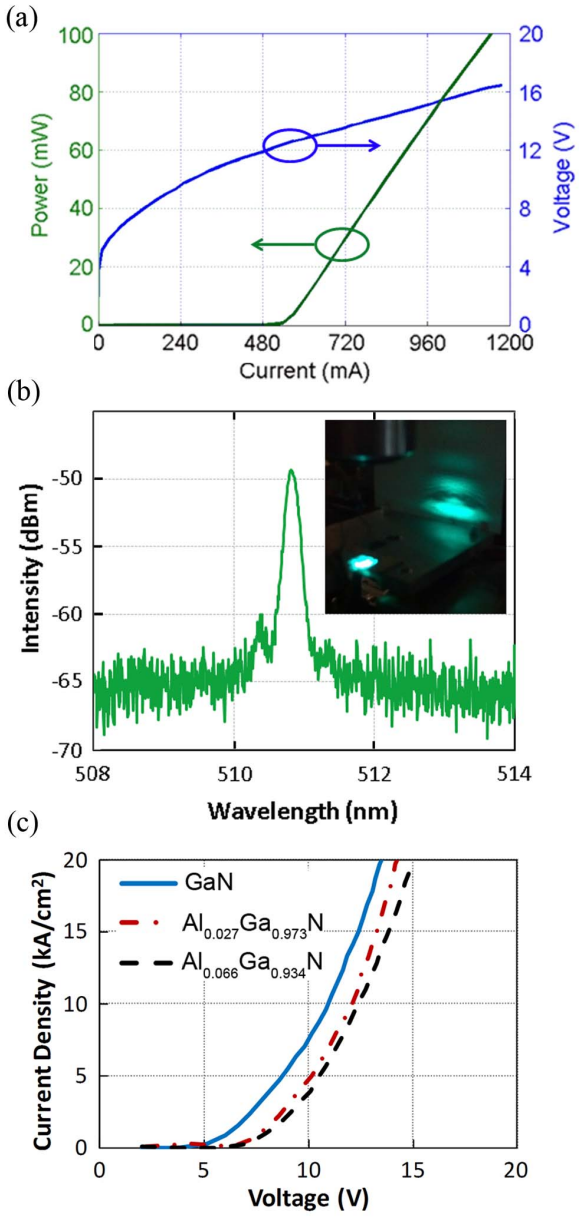

Fig. 5. (a) Light–current–voltage characteristics for a 2 μm wide, 1800 μm long uncoated etched facet laser diode employing GaN barriers, (b) lasing spectra just above threshold with a far-field pattern inset, and (c) current density–voltage curves for LDs with different $Al_yGa_{1-y}N$ barrier compositions.

of defects originate in the QWs. The average void diameter is approximately 50 nm.

Figure 5 gives the light–current–voltage characteristics of a 2 μm wide by 1800 μm long uncoated etched facet LD from the sample with GaN barriers. Spectra and far-field pattern (inset) are given in Fig. 5(b), showing lasing at 510.7 nm with a full-width at half-maximum of 0.18 nm. Measurements were taken with a pulse length of 1.2 μs and a duty cycle of 0.36 %. Threshold current and voltage were 540 mA and 12.4 V, respectively, giving J_{th} of 15 kA/cm^2 with a slope efficiency of 0.17 W/A and up to 100 mW optical output power out of each uncoated facet. The device with an $Al_yGa_{1-y}N$ barrier composition of $y = 0.027$ had a J_{th} of 47 kA/cm^2, and the device with $y = 0.066$ did not lase. Current density–voltage characteristics of the barrier composition series are given in Fig. 5(c). The GaN barrier LD had the lowest turn-on voltage, and voltage increased with increasing barrier AlN fraction.

IV. Discussion

From Fig. 2, DTDs are related to post-QW thermal damage—DTDs are not present without post-QW annealing, and their size increases with anneal time. The anneal temperature series in Fig. 3 also shows a correlation of DTD size with thermal damage. As the p-GaN temperature decreased from 920 °C to 840 °C the maximum defect size decreased from over 1 mm to 250 μm. Once formed, increase in DTD size is driven by both anneal temperature and time. However, in both cases there was no correlation with DTD density. Thermal damage does not appear to control the nucleation behavior for these defects, but rather influences their rate of growth.

Defects with similar morphology and microstructure have been observed for green (20$\bar{2}\bar{1}$) LEDs [12]. For this

system, a reduction of DTD density was achieved by reducing QW growth rate. However, a similar approach has not proved effective for $(20\bar{2}1)$ grown QWs at this point. For both $(20\bar{2}1)$ and $(20\bar{2}\bar{1})$, DTD densities are on the order of 10–10^3 cm^{-2} and the void density within the DTD region is on the order of 10^9 cm^{-2}. Neither DTD nor void densities correlate well with known extended defect densities, such as threading dislocations (5×10^6 cm^{-2}). The physical origin and formation mechanism of DTDs are still under investigation.

The TEM image in Fig. 4 shows both voids and BPSFs originating in the QWs in the DTD region of a LD sample. In this region, the void density was on the order of 10^9 cm^{-2}. The stacking faults propagate out of regions both with and without voids, and are not necessarily correlated with void formation. However BPSFs are generally not observed outside of the DTD regions for $(20\bar{2}1)$ green LD structures in the wavelength range discussed above. The voids formed by thermal damage, along with the BPSFs, lead to complete quenching of radiative emission in the DTD regions and prevent LD operation. Further analysis of the structure of these voids can be found in Ref. [12].

The realization of usable GaN clad LD structures with GaN barriers is enabled by reduced p-GaN growth temperature, as discussed above. The AlGaN barrier LD series showed substantially reduced J_{th} with lower AlGaN content in the barriers, likely due to the increase of Γ as discussed above. Higher Γ structures having low index AlGaN, AlInN or quaternary AlInGaN cladding would show reduced dependence of Γ on the barrier composition. For structures with low index cladding, the cladding layer rather than the active region would then play the dominate role in waveguiding. However, AlGaN cladding layers typically relax before useful thicknesses/compositions can be realized [13], [14] and it can be difficult to grow high quality low resistance p-type AlInN and AlInGaN cladding layers at temperatures low enough to incorporate a significant amount of InN [15].

The voltage of the processed LD samples increased with barrier AlN fraction, as seen in Fig. 5(c). There is a clear increase in turn-on voltage for devices with AlGaN barriers. Increased voltage could be due to poor carrier transport between QWs in the active region due to increasing barrier height with higher AlN fraction. In addition, the affinity of AlGaN for oxygen has been well established, especially when grown at low temperature [16]. AlGaN containing barriers could increase oxygen contamination in the active region and change junction location. The overall high voltage is likely due to relatively unoptimized contacts and doping, as well as the low temperature grown p-GaN.

V. Conclusion

We have shown DTDs in green semipolar $(20\bar{2}1)$ QWs are related to post-QW thermal damage. The size of DTDs can be suppressed by reducing the temperature and growth time of the subsequently grown p-type layers, although this does not appear to impact DTD density. From TEM investigations, the DTDs are comprised of BSPFs and approximately 10^9 cm^{-2} voids. Suppression of DTD formation without the need for AlGaN barriers allowed a direct comparison of green regime LDs with GaN and AlGaN barriers. 511 nm LDs with GaN barriers showed a significant reduction of J_{th} relative to AlGaN barrier devices. GaN clad LDs with GaN barriers have significantly higher Γ than similar LDs with AlGaN containing barriers, while avoiding oxygen contamination and other issues associated with low temperature AlGaN growth within the active region.

References

[1] S.-H. Park and D. Ahn, "Depolarization effects in $(11\bar{2}2)$-oriented InGaN/GaN quantum well structures," *Appl. Phys. Lett.*, vol. 90, no. 1, pp. 013505-1–013505-3, 2007.

[2] W. G. Scheibenzuber, U. T. Schwarz, R. G. Veprek, B. Witzigmann, and A. Hangleiter, "Calculation of optical eigenmodes and gain in semipolar and nonpolar InGaN/GaN laser diodes," *Phys. Rev. B*, vol. 80, no. 11, pp. 115320-1–115320-16, 2009.

[3] D. Sizov, R. Bhat, and C.-E. Zah, "Gallium indium nitride-based green lasers," *J. Lightw. Technol.*, vol. 30, no. 5, pp. 679–699, Mar. 1, 2012.

[4] S. Takagi, *et al.*, "High-power (over 100 mW) green laser diodes on semipolar $\{20\bar{2}1\}$ GaN substrates operating at wavelengths beyond 530 nm," *Appl. Phys. Express*, vol. 5, no. 8, pp. 082102-1–082102-3, 2012.

[5] J. W. Raring, *et al.*, "High-efficiency blue and true-green-emitting laser diodes based on non-*c*-plane oriented GaN substrates," *Appl. Phys. Express*, vol. 3, no. 11, pp. 112101-1–112101-3, 2010.

[6] Y.-D. Lin, *et al.*, "High quality InGaN/AlGaN multiple quantum wells for semipolar InGaN green laser diodes," *Appl. Phys. Express*, vol. 3, no. 8, pp. 082001-1–082001-4, 2010.

[7] A. Avramescu, *et al.*, "InGaN laser diodes with 50 mW output power emitting at 515 nm," *Appl. Phys. Lett.*, vol. 95, no. 7, pp. 071103-1–071103-3, 2009.

[8] *Photon Design, FIMMWAVE Version 5.3.2*, Photon Design, Oxford, U.K., 2011.

[9] M. J. Bergmann and H. C. Casey, "Optical-field calculations for lossy multiple-layer $Al_xGa_{1-x}N/In_xGa_{1-x}N$ laser diodes," *J. Appl. Phys.*, vol. 84, no. 3, pp. 1196–1203, 1998.

[10] N. A. Sanford, *et al.*, "Refractive index study of $Al_xGa_{1-x}N$ films grown on sapphire substrates," *J. Appl. Phys.*, vol. 94, no. 5, pp. 2980–2991, 2003.

[11] A. Saxler, W. C. Mitchel, P. Kung, and M. Razeghi, "Aluminum gallium nitride short-period superlattices doped with magnesium," *Appl. Phys. Lett.*, vol. 74, no. 14, pp. 2023–2025, 1999.

[12] Y. Zhao, *et al.*, "Suppressing void defects in long wavelength semipolar $(20\bar{2}\bar{1})$ InGaN quantum wells by growth rate optimization," *Appl. Phys. Lett.*, vol. 102, no. 9, pp. 091905-1–091905-4, 2013.

[13] A. Tyagi, *et al.*, "Partial strain relaxation via misfit dislocation generation at heterointerfaces in (Al,In)GaN epitaxial layers grown on semipolar $(11\bar{2}2)$ GaN free standing substrates," *Appl. Phys. Lett.*, vol. 95, no. 25, pp. 251905-1–251905-3, 2009.

[14] A. E. Romanov, *et al.*, "Basal plane misfit dislocations and stress relaxation in III-nitride semipolar heteroepitaxy," *J. Appl. Phys.*, vol. 109, no. 10, pp. 103522-1–103522-12, 2011.

[15] R. Butté, *et al.*, "Current status of AlInN layers lattice-matched to GaN for photonics and electronics," *J. Phys. D, Appl. Phys.*, vol. 40, no. 20, pp. 6328–6344, 2007.

[16] C. Moe, *et al.*, "Increased power from deep ultraviolet LEDs via precursor selection," *J. Cryst. Growth*, vol. 298, pp. 710–713, Jan. 2007.